CrossMark

Electrochemical Corrosion Behaviour of Ti–29Nb–13Ta–4.6Zr Alloy in Physiological Solution Containing Various Synovial Joint Lubricants

N. S. More[1] · S. N. Paul[2] · Manish Roy[3]

Abstract

Ti alloys are well known for their biocompatibility and high specific strength. In the present work, the electrochemical behaviour of Ti–13Ta–29Nb–4.6Zr alloy having β structure in Hank's solution containing various joint lubricants has been studied. The results show that Ti–13Ta–29Nb–4.6Zr alloy is a potential biomaterial for joint applications. The electrochemical behaviour of Ti–13Ta–29Nb–4.6Zr alloy is not influenced significantly by the nature of lubrication. The highest corrosion rate of investigated alloy is around 1.2 mm/year in Hyaluronic Acid containing Hank's solution. The growth of passive layer is the slowest and the passive layer is the most porous in Hank's solution containing hyaluronic acid.

Keywords Titanium · Electrochemical Impedance Spectroscopy (EIS) · Polarization · Potentiostatic · Passivity

1 Introduction

Ti-based alloys are extensively used in biomedical applications. The widespread use of Ti alloys as biomaterials is because of their excellent corrosion resistance, high specific strength and high specific stiffness [1]. Spontaneous formation of passive titanium dioxide (TiO_2) film, typically few nanometer thick, is responsible for their biocompatibility. Initially, α and α + β alloys such as Ti and Ti–6Al–4V were employed as various dental and orthopaedic implants. However, the unsuitability of these alloys for load-bearing applications [2], led to development of high-purity alloy. The release of aluminium and vanadium ions was found to be toxic and their accumulation in the surrounding body was of great concern [3]. Consequently, effort was diverted towards development of Ti-based biomaterials free from Al and V. Further, it is noted that these α or α + β alloys have elastic modulus significantly higher than the elastic modulus of implant and bone. In order to overcome this drawback, β

Ti alloys were developed with the aid of β stabilizing elements such as Nb, Mo, Zr and Ta. β Ti alloys were found to have enhanced biocompatibility and increased compatibility with the mechanical properties of bone and implants [4].

Over the last decades, an extensive research [5–21] has been carried out on the electrochemical behaviour of various Ti alloys in physiological environment. Most of these studies are concerned with open circuit potential study, potentiodynamic study, cyclic polarization study and electrochemical impedance spectroscopy (EIS) study with Nyquist and Bode plot in artificial physiological solution such as Hank's solution and Ringer's solution. Materials used in these studies are C.P. Ti [15, 18], Ti–6Al–4V [7, 20], Ti–48Al–2Cr–2Nb [15, 21], Ti–15Mo, Ti–29Nb–13Ta–4.6Zr, NiTi, Ti–Hf, Ti–15Al, Ti–13.4Al–29Nb, Ti–7Nb–6Al [9, 20], Ti–13Nb–13Zr [7, 9, 15], Ti–15Zr–4Nb [9], Ti–12Mo–5Ta, Ti–Ta–Zr [10], TiMoZrTa [8], etc. The corrosion behaviour of all these Ti alloys was found to be generally similar. Most of these alloys passivate spontaneously in simulated body fluid. These alloys exhibit very low susceptibility to pitting corrosion. These studies reveal the presence of single- or double-layer passive film on these alloys. The physico–chemical and electrochemical characteristics of the oxide film and its long-term stability in biological solution eventually determine the corrosion properties. Further, it was noted in earlier studies that the presence of lubricant in synovial constituent changes the tribo-corrosion behaviour of beta Ti alloys significantly [22–24]. Based on such observation, it

✉ N. S. More
nshirish@npcil.co.in

1 Present Address: Nuclear Power Corporation of India Limited, Mumbai 40094, India

2 Visvesvaraya National Institute of Technology, Nagpur 440012, India

3 Defence Metallurgical Research Laboratory, PO: Kanchanbagh, Hyderabad 500058, India

was contemplated that lubricant will influence the corrosion behaviour. However, hitherto no reported result is available on the influence of lubricant that exists in joint, on the corrosion behaviour of these alloys even though these materials are serious contender for joint replacement application. In view of the above, the present research is undertaken to understand the effect of lubricant on the failure mechanism of Ti–13Ta–29Nb–4.6Zr alloy in lubricant containing Hank's solution. This paper presents results obtained by open circuit potential, potentiodynamic study and impedance spectroscopy study of the above-mentioned Ti alloy in Hank's solution containing three different types of lubricants namely, dipalmitoylphosphatidylcholine (DPPC), bovine serum albumin and hyaluronic acid. The corrosion data were interpreted with most probable impedance (MPI) equivalent circuit diagram.

2 Experimental Details

2.1 Materials and Methods

The material used in the present study is Ti–13Ta–29Nb–4.6Zr alloy. This alloy is free from V and Al. This material was prepared by melting in vacuum arc electric furnace (non-consumable) and casting in the form of pancakes followed by forging. A vacuum arc electric furnace in which charge can be melted on a water-cooled copper crucible under vacuum 10^{-3} mbar was employed. Prior to melting, the furnace chamber was purged with argon gas once and then it was filled with the gas again up to 532 mbar. The charge was melted by arcing emitted from a tungsten bit brazed to copper stringer rod suspended above the charge. A DC potential of up to 30–32 V and a current 1000 Å was applied between tungsten cathode and charge material, which formed the anode. A stirring coil around the copper crucible stirred the melt pool and homogenized the melt composition. Each pancake was melted four times to homogenize. The pancake was then forged in a forging press. Elemental analysis of the test materials was done using inductively coupled plasma optical emission spectrophotometer (ICP–OES). Interstitial elements were detected by LECO oxygen, nitrogen analyser. The measured composition of the test materials is given in Table 1. Vickers's hardness of these materials was measured using a macrohardness tester (Wolpert, Germany) with a load of 10 kg held for 15 s. The diffraction pattern of this alloy was obtained from Philips diffractometer (Model No. PW3020).

2.2 Corrosion Testing

Specimens of dimension 20 mm × 20 mm were taken for electrochemical studies. Sample preparation was done by

Table 1 Chemical composition of Hank's solution

Chemicals	g/l (pH 7.8)
NaCl	8
KCl	0.4
$CaCl_2$	0.14
$MgSO_4 \cdot 7H_2O$	0.06
$NaHCO_3$	0.35
NaH_2PO_4, H_2O	0.143
D-Glucose	1
$KH2PO_4$	0.6
$MgCl_2 \cdot 6H_2O$	0.1

Table 2 Composition and hardness of the test material

Element	Composition
C (wt%)	0.05
S (wt%)	0.05
H_2 (ppm)	230
Nb (wt%)	27.2
Ta (wt%)	11.5
Zr (wt%)	4.8
Ti (wt%)	Bal
Hardness (HV)	221

progressively polishing with emery papers of 240, 400 and 500 grit, followed by fine polishing with diamond paste (6 μm) and final polishing with alumina powder (3 μm) in KOH solution. The specimens were then washed in deionised water and ultrasonically cleaned in acetone and ethanol for 10 min, respectively. The area to be exposed for electrochemical studies was 1×1 cm^2.

The used electrolytes simulate human body fluid condition. This is essentially Hank's solution, the composition of which is given in Table 2 [25].

1. Hank's balanced salt solution (HBSS) + 4 g/l bovine serum albumin (BSA)
2. HBSS + 3 g/l dipalmitoylphosphatidylcholine (DPPC)
3. HBSS + 3 g/l hyaluronic acid (HA)
4. HBSS + 4 g/l BSA + 3 g/l HA

These solutions were prepared using laboratory grade chemical and distilled water. Lubricants are obtained from 'Sigma Aldrich'. The electrochemical studies were conducted using Autolab ecochemie PGSTAT 302 potentiostat, interfaced to a personal computer. Electrochemical polarization studies were conducted in a flat electrochemical cell (Friction and wear tech, Chennai) in de-aerated condition by nitrogen purging. The potential of the working electrode was measured against Ag/AgCl (3 M KCl) reference electrode. The Luggin capillary was placed close to the working electrode. Pt wire was used as auxiliary electrode.

All the potentiodynamic polarization studies were carried out after stabilization of the open circuit potential (OCP). The scan rate used was 2 mV/s. The corrosion rate was determined using Tafel extrapolation method, as per ASTM standard G5. The Tafel slope cathodic (β_c) and anodic (β_a) and the corrosion current densities (i_{corr}) were estimated from the Tafel plots. Tafel slope is the ratio of overpotential vs. current density for both anodic and cathodic curve. The corrosion rates were obtained from the corrosion current density using Faraday's law.

Alternate current (AC) impedance spectra were obtained using the same instrument. The scan frequency range was set at 300 kHz–10 mHz with perturbation amplitude of 10 mV. The barrier layer resistance (R_Q) from AC spectra analysis was obtained by using the frequency response analyser (FRA) software. EIS studies on samples were performed at their respective equilibrium potentials (OCP). Impedance measurements were made at a higher frequency range by performing the lock-in experiment, followed by a fast Fourier transform (FFT) experiment, which measures the impedance in the lower frequency range. In the lock-in experiment, the impedance of the sample was measured by imposing an AC voltage perturbation (sine wave), measuring the AC current and voltage within the lock-in, then calculating the impedance at a particular frequency. The upper limit of the frequency was 1×10^4 Hz and the lower limit was 0.1 Hz.

3 Results and Discussion

3.1 Materials Characterization

The present investigation is carried out using Ti–13Ta–29Nb–4.6Zr alloy having β structure. This material is free from vanadium and so there is no problem of
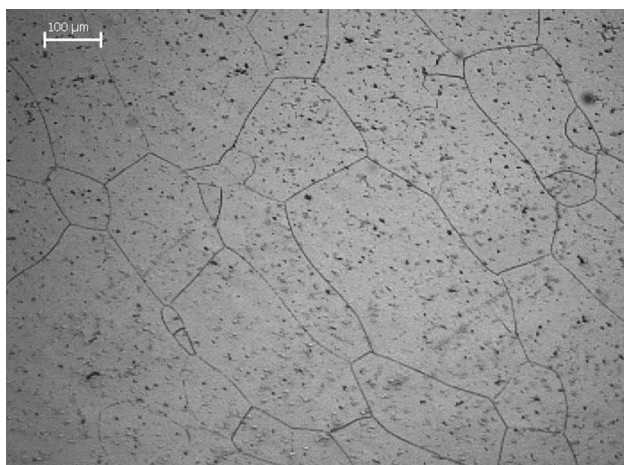

Fig. 1 Optical micrograph of the test material

vanadium toxicities. Table 2 indicates that the measured composition of Ti–13Ta–29Nb–4.6Zr differs marginally from the nominal composition. The amount of Nb and Ta, which are heavier than Ti, are found to be less than nominal composition. The microstructure of the test material is documented in Fig. 1. It can be seen that single-phase β microstructure having around 200 µm grain size is the main feature of the microstructure of Ti–13Ta–29Nb–4.6Zr alloy. The XRD pattern obtained from the test material is given in Fig. 2. The XRD pattern confirms single-phase β structure.

3.2 Corrosion Behaviour

The variation of current with time at 0.1 V versus Ag/AgCl anodic potential of the said alloy in Hank's solution containing BSA, BSA and HA and DPPC is presented
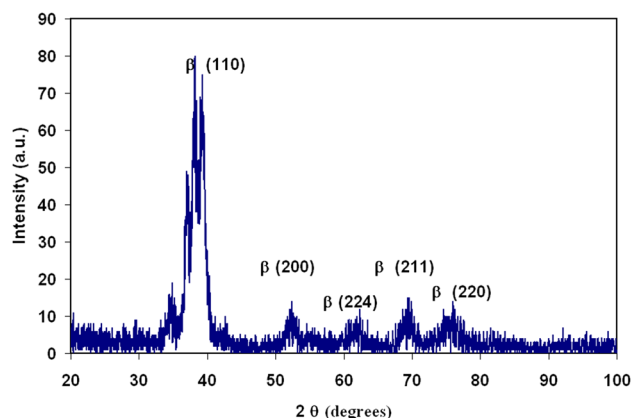

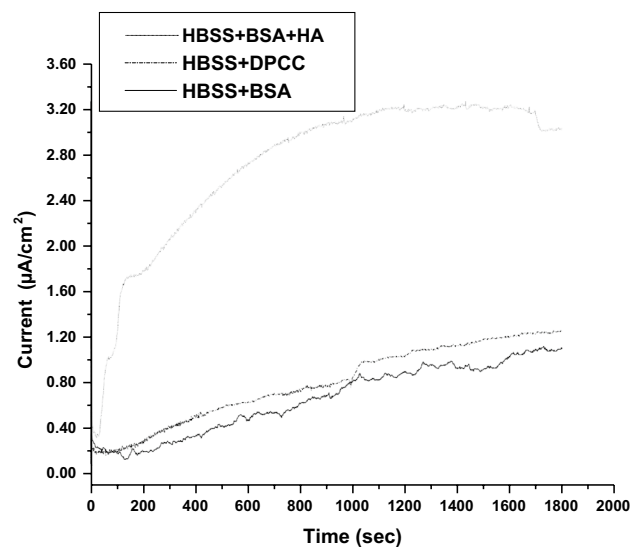**Fig. 2** The XRD pattern of the test material

Fig. 3 The current at open circuit potentials of the tested alloys in Hank's solution containing BSA, BSA and HA and DPPC

in Fig. 3. Test was conducted up to 1800 s. It is clear that Ti–13Ta–29Nb–4.6Zr alloy cannot form passive layer in Hank's solution containing BSA or DPPC. But it can form passive layer in Hank's solution containing BSA and HA lubricant after around 1000 s. It should be stated that the corrosion current of the investigated alloy in Hank's solution with BSA and HA is nearly three times higher than that in Hank's solution containing either BSA or DPPC.

The variation of corrosion current for the test material with potential in different electrolytes is given in Fig. 4. These curves are similar in nature for all electrolytes and essentially show behaviour typical to that of Ti alloy. The polarization curves show four potential domains. The first domain is cathodic domain, which includes all potential below the corrosion potential. In this domain, current is determined by reduction of protons and water and to a less extent, oxygen. The second domain pertains to potential range between corrosion potential and around 0.5 V. This domain is transition from cathodic to anodic current at corrosion potential. Since there is no fluctuation in corrosion currents it can be concluded that this material passivates spontaneously in solution. Thus, corrosion potential is directly located in passive region. The third domain corresponds to passive plateau between 0.5 V and transpassive potential. In this domain, passive film forms and it impedes the dissolution of metal and reduces the corrosion rate. The fourth domain is the transpassive region where current increases abruptly with increase of potential. This domain cannot be seen within the experimental regime for most of the electrolytes. However, this domain starts at around 3.5 V for HBSS solution containing HA. Thus, in this solution, transpassivity is due to oxidation of water freeing the molecular oxygen. In other solution, oxygen evolving over potential is too high to allow this process to take place. It is to be stated that all the polarization curves are fairly reproducible.
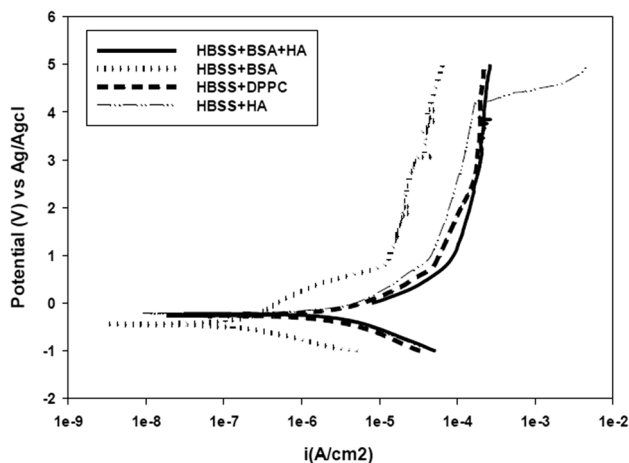

Fig. 4 The variation of corrosion current for the test material with potential in Hank's solution containing BSA, BSA and HA and DPPC

The passive range of this alloy is very large indicating excellent stability of these passive films in all electrolytes. The potentiodynamic polarization indicates that passivation process is spontaneous and not electrochemical. Significant parameters such as OCP, I_{CORR}, corrosion rate, cathodic and anodic Tafel slope obtained in different solution are listed in Tables 3 and 4 The corrosion current density ($\mu A/cm^2$) is determined by employing Tafel extrapolation [26] as given below.

$$I_{CORR} = \frac{\beta_a \beta_c}{2.3 R_P (\beta_a + \beta_c)} \tag{1}$$

The corrosion rate was determined by the following equation:

$$\text{Corrosion rate (mm/y)} = \frac{0.00327 \times I_{CORR} \times M_W}{n \times d}, \tag{2}$$

where M_W is the molar weight, n is valency and d is the density in g/cm^3 of the corroding species. The corrosion current is high for HBSS containing Hyaluronic acid and the polarization resistance is least for HBSS containing bovine serum albumin.

The enhanced passivation of the test material can be attributed to the presence of significant amount of Nb in the alloy. Nb cation improves the passivation properties of the film by decreasing the concentration of the anion vacancies in the TiO_2 film. These anion vacancies are generated by the presence of lower titanium oxide states [27]. The effect of

Table 3 The open circuit potential (OCP), corrosion current density (I_{CORR}) and polarization resistance (R_P) of Ti–29Nb–13Ta–4.6Zr alloy tested in Hank's solution containing various lubricant for 1 h at 298 K

Solution	OCP (V vs. Ag–AgCl)	I_{CORR} ($\mu A/cm^2$)	R_P (Ohm)
HBSS + BSA	− 0.34	2.8 ± 0.2	$(54.5 \pm 5.0) \times 10^4$
HBSS + HA	− 0.18	5.9 ± 0.6	$(2.8 \pm 0.3) \times 10^4$
HBSS + BSA + HA	− 0.30	3.3 ± 0.3	$(5.8 \pm 0.6) \times 10^4$
HBSS + DPPC	− 0.19	3.9 ± 0.4	$(3.0 \pm 0.2) \times 10^4$

Table 4 The cathodic Tafel slope, anodic Tafel slope and corrosion rate of Ti–29Nb–13Ta–4.6Zr alloy tested in Hank's solution containing various lubricants for 1 h at 298 K

Solution	β_c (V/decade)	β_a (V/decade)	Corrosion rate (mm/year)
HBSS + BSA	0.42	0.31	0.6 ± 0.05
HBSS + HA	0.38	0.37	1.2 ± 0.08
HBSS + BSA + HA	0.40	0.42	0.7 ± 0.05
HBSS + DPPC	0.34	0.29	0.8 ± 0.05

Nb addition as alloying element in stabilizing surface film for Ti alloy has previously been reported [28]. The presence of Ta in the alloy will be responsible for the formation of protective anodic Ta_2O_5 oxide. This oxide may stay as crystalline oxide or amorphous oxides depending on the corrosion conditions. In general, they exist in glassy state. This oxide can be crystallized by thermal crystallization [29] or by electric crystallization [30]. According to Leach and Pearson [31], growth of crystalline oxide is generally favoured when an amorphous oxide is under compressive stress. Previous studies did indicate that Ta exhibits better corrosion resistance than Ti in various corrosive mediums [32]. It is also noted that unrecrystallized structure has higher corrosion rates than crystallized structure [33]. Thus, the presence of crystallized anodic Ta_2O_5 oxide is expected to improve corrosion resistance of the investigated alloy. Previous study using XPS indicated that during corrosion of Zr containing Ti alloy in physiological solution, Zr tends to diffuse to the surface of the alloy [34]. Zr has a tendency to form very protective passive layer giving rise to lower corrosion rate.

Figure 5 shows the Nyquist plot of the investigated materials in Hank's solution containing HA and DPPC. The spectra exhibit incomplete semicircle with single time constant in spite of the fact that most Ti alloys exhibit spectra with two time constants in physiological solution [35]. This is an indication of highly capacitive behaviour even though it is very
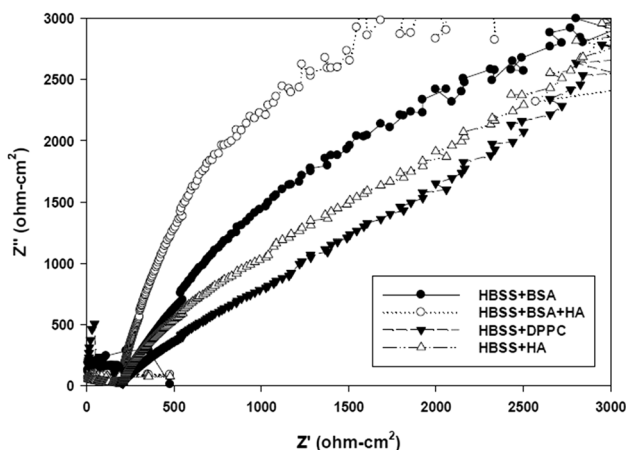
difficult to interpret such incomplete Nyquist plot. The data from Nyquist plot are analysed to determine solution resistance (R_S), the resistance of the barrier layer at the electrode/solution interface and the capacitance of the barrier layer at the interface. These parameters are obtained by curve fitting EIS data using FRA software in Autolab. The resistance of the barrier layer at the electrode/solution interface (R_Q) is calculated from the difference in the impedance at lower and higher frequencies as suggested by Tsuru et al. [36]. The capacitance of barrier layer is obtained as

$$C_Q = \frac{1}{\left\{2\pi f\left(-Z''_{max}\right)\right\}^p R_Q}, \tag{3}$$

where $-1 < p < 1$. The value of n is associated with the non-uniform distribution of current as a result of roughness and surface defects [27, 37]. These parameters are listed in Table 5. Based on visual observation and impedance spectra, the corrosion behaviour is modelled by equivalent circuit as depicted in Fig. 6. In Fig. 6, C_Q, R_S, and R_Q represent capacitance of passive film, solution resistance and polarization resistance, respectively. This model for single passive layer is nearly same in all solution. It is to be noted that addition of synovial constituents results in an increase in solution resistance. From Table 5, it can be stated that R_Q is the highest in Hank's solution containing DPPC and it is the least in Hank's solution with BSA and HA. This feature can be attributed to the fact that the alloy forms most porous film in the solution containing BSA and HA. The double-layer capacitance is in the range of 3.4–5.7 μF/cm². These values are little higher than the values reported by Assis et al. [17] for other Ti alloys in Hank's solution, lower than the values of various heat-treated Ti–6Al–4V alloy and comparable to
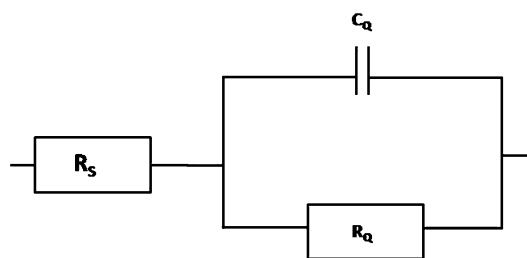

Fig. 5 The Nyquist plot of the investigated materials in Hank's solution containing HA and DPPC

Fig. 6 The equivalent circuit diagram of the corrosion behaviour of investigated materials in hank solutions containing HA and DPPC

Table 5 Important parameters determined from Nyquist plot for the test material in Hank's solution containing various lubricants	Solution	R_S (Ωcm²)	C_Q (μF/cm²)	p	R_Q (kΩ cm²)	Chi square
	HBSS + BSA	307.0	4.61	0.85	1.0	0.05
	HBSS + HA	187.0	3.40	0.85	1.0	0.04
	HBSS + BSA + HA	252.3	5.72	0.89	0.4	0.06
	HBSS + DPPC	243.8	4.25	0.69	2.7	0.07

the values of various heat-treated Ti–48Al–2Cr–2Nb alloy in Ringer's solution [21]. It is least for the solution containing HA. A low value of C_Q corresponds to slow growth of oxide film indicating long-term stability of the oxide film of the alloy in Hank's solution containing HA

The value of p in the middle frequency range varies between 0.69 and 0.89 and is associated with the non-uniform distribution of current as a result of roughness and surface defects. These values are consistent with that reported by Hsu et al. [38] for Ti–6Al–4V alloy in phosphate buffer solution and Assis et al. [17] for various Ti alloys in Hank's solution. The value of p is the minimum for Hank's solution containing DPPC lubricant and it is the maximum for Hank's solution having BSA and HA. The p value being close to 1 for the investigated materials suggests that the behaviour of the passive layer approaches to that of an ideal capacitor [38]. p value close to 0.5 is indicator of Warburg impedance. Thus, the material behaves more like Warburg impedance in HBSS solution containing DPPC indicating that the corrosion rate is governed by diffusion of corroding species in the electrolyte. Hence, R_Q is highest in HBSS containing DPPC although the least corrosion rate is observed in HBSS containing BSA. In all other electrolytes (HBSS containing BSA, HA, BSA + HA), it exhibits capacitive response.

The results of impedance spectroscopy are shown in Figs. 7 and 8 in the form of Bode impedance and phase angle diagram. In all four solutions, a highly capacitive behaviour typical of passive materials is noted. The Bodo diagrams, which are due to barrier layer characteristics, reveal the presence of two distinct regions. In the high frequency region (1–100 kHz) Bode plot exhibits constant log|Z| versus log(f). In this region, phase angle approaches 0°. This is due to electrolyte resistance R_s and this region can be termed as resistive region. In the high frequency region, solution resistance
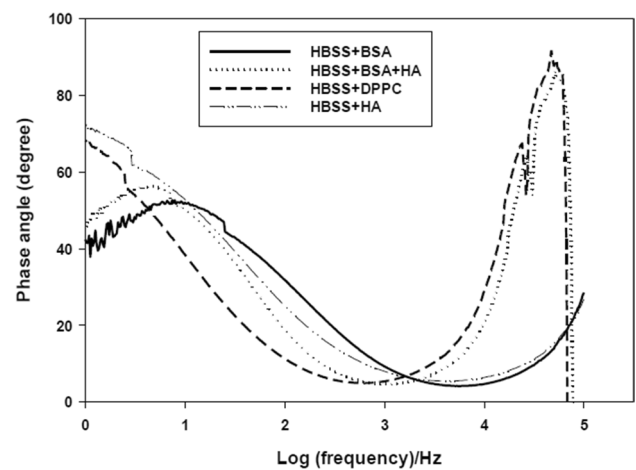
Fig. 8 The results of impedance spectroscopy of the investigated alloys in the form of phase angle diagram tested in Hank's solutions containing various joint lubricants

of the electrolyte dominates the corrosion behaviour of the materials. In the low and medium frequency region, log|Z| versus log(f) decreases with a linear slope around −0.9. In this region, phase angle value approaches 90°. This is characteristics response of compact passive oxide capacitance of Ti alloys and this region is identified as capacitive region. The high impedance at low frequency suggests high corrosion resistance. These results support passive behaviour of investigated alloy in physiological solution containing synovial lubricants in conformity with the potentiodynamic behaviour. As the phase angles approached to 90°, the formation of a highly stable film is indicated in all the electrolytes used [8, 39]. This is consistent with the low corrosion rates determined in the potentiodynamic test. These plots also show single time constant implying formation of a single-layer passive film. Further, the nature of Bode plots is more or less similar in all solutions.

The scanning electron microscopy (SEM) micrographs showing the morphology of corroded surfaces of the sample obtained from Hank's solution containing BSA + HA and Hank's solution with only BSA are presented in Fig. 9 and the energy dispersive analysis of X-rays (EDAX) spectra obtained from those surfaces are given in Fig. 10. It is clear that the presence of BSA and HA causes high and uniform reaction in conformity with the findings of open circuit potential. Small pits can be seen all over the corroded surface for the specimen immersed in Hank's solution containing only BSA. Thus, the presence of BSA may cause pitting in this material even though such process has not been noted in potentiodynamic polarization curves and this material has excellent pitting resistance in physiological solution. On the contrary, when both HA and BSA are present in Hank's solution, a complete uniformly reacted surface can be seen. The compositions of the corroded surfaces as obtained from
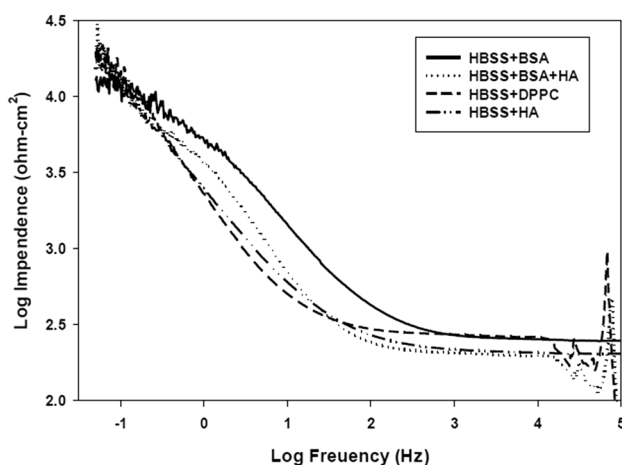

Fig. 7 The results of impedance spectroscopy for tested materials in the form of Bode impedance tested in Hank's solutions containing various joint lubricants
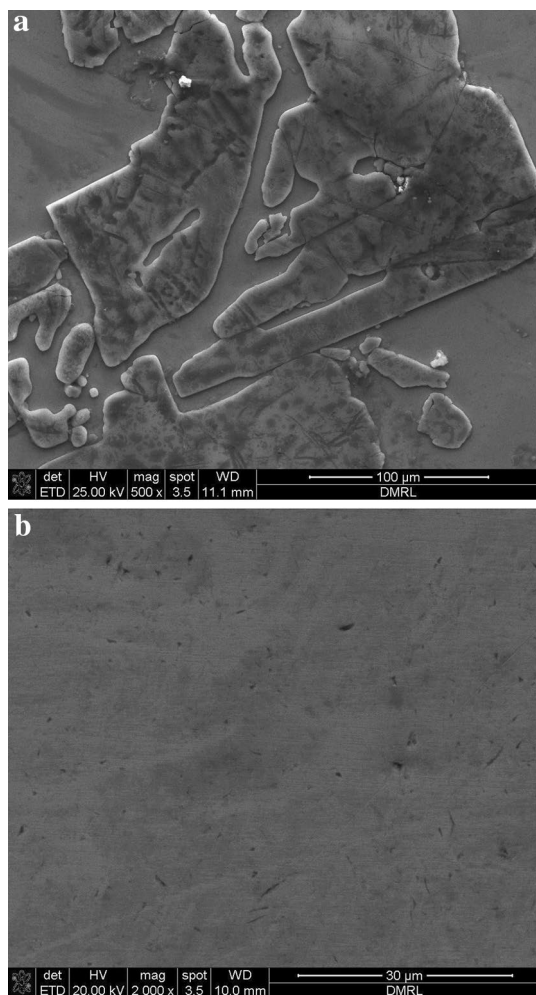
Fig. 9 The SEM micrographs showing the morphology of corroded surfaces of the sample. **a** Hank's solution containing BSA+HA, **b** Hank's solution with only BSA
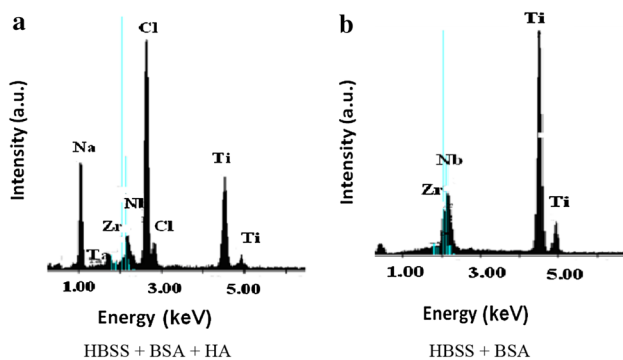

Fig. 10 The EDAX spectra of the corroded surfaces. **a** Hank's solution containing BSA+HA, **b** Hank's solution with only BSA

Table 6 Composition of the surfaces as measured by EDS corroded in two different physiological solutions containing different lubricants for 1 h at 298 K

Solutions	HBSS + BSA	HBSS + BSA + HA
Elements	Wt%	Wt%
O	14.6	4.7
Na		22.5
Ta	2.1	7.7
Zr		3.0
Nb	15	9.4
C		34.3
Ti	68.1	18.3

corroded surface of the test specimen immersed in Hank's solution containing BSA and HA. They can be due to deposition of recrystallized salt.

As mentioned previously, the passive layer that forms on the tested alloy in the Hank's solution containing HA has least value of barrier layer capacitance (C_Q) signifying slow growth of the passive layer. Further, the solution resistance of this alloy in Hank's solution containing HA is least and the potentiodynamic curves exhibit the highest corrosion rates in the same solution due to high porosity in the passive layer. Thus, the passive layer is grown not only slowly but also most porous in Hank's solution containing HA. Such porous layer displays better osseointegration [40]. Migration of the bone cells present in the body environment into the pores of the passive films facilitating adhesion between the plant and bone is considered to be the reason for improved osseointegration. Further, it is to be stated that corrosion rate is lowest in BSA containing solution. One reason is the formation of compact passive layer. Secondly, albumin binds with water, K^+, Na^+ and Ca^+ ions, which are the main components of Hank's solution, and thus reduces corrosion rates. The presence of hyaluronic acid leads to the formation of porous layer, which allows relatively easy movement of corrosion species across the layer, and increase of corrosion rates.
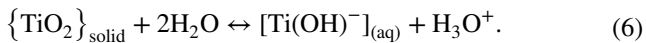
3.3 Corrosion mechanisms of Ti–10V–2Fe–3Al in Hank's solution

Titanium surface covered by a natural oxide film has been studied in a variety of physiological solution. Dissolution of the titanium oxide film in water can be represented by the following reaction:
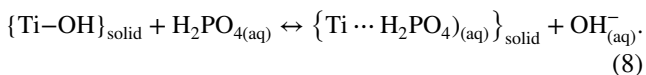
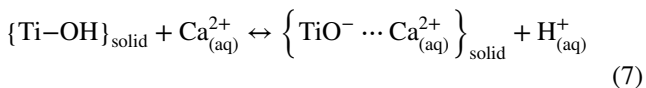$$TiO_2 + 2H_2O \leftrightarrow Ti(OH)_4. \tag{4}$$

The presence of a small amount of corrosion products is expected to induce minimal unwanted biochemical

energy dispersive spectroscopy (EDS) spectrum are listed in Table 6. A high amount of Na and Cl can be seen on the

reactions such as strong protein binding and unfolding as the majority of the dissolved species has been noted to be uncharged. Thus, Eq. (4) leads to

$$\{TiO_2\}_{solid} + 2H_2O \leftrightarrow [Ti(OH)_3]^+_{(aq)} + OH \tag{5}$$

$$\{TiO_2\}_{solid} + 2H_2O \leftrightarrow [Ti(OH)^-]_{(aq)} + H_3O^+. \tag{6}$$

The calcium ions present in the SBF solution tend to attach to the titanium oxide surface upon immersion. The concentrations of calcium and phosphate ions at the surface and therefore the thickness of the calcium phosphate were observed to increase with the immersion time:

$$\{Ti-OH\}_{solid} + Ca^{2+}_{(aq)} \leftrightarrow \left\{TiO^- \cdots Ca^{2+}_{(aq)}\right\}_{solid} + H^+_{(aq)} \tag{7}$$

$$\{Ti-OH\}_{solid} + H_2PO_{4(aq)} \leftrightarrow \left\{Ti \cdots H_2PO_{4}{}_{(aq)}\right\}_{solid} + OH^-_{(aq)}. \tag{8}$$

Equation (7) shows the influence of cations (Ca^{2+}, Mg^{2+}) adsorption on the surface and Eq. (8) shows the exchange of basic hydroxide anions (OH−) with phosphate anions:

$$3Ca^{2+}_{(aq)} + 2PO_4^{3-}_{(aq)} \leftrightarrow \left\{Ca_3(PO_4)_{2solid}\right\}. \tag{9}$$
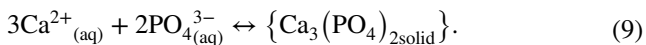
4 Conclusions

1. The kinetic parameters (E_{corr} and I_{corr}) obtained from potentiodynamic technique indicate fairly good corrosion resistance of the alloy Ti–29Nb–13Ta–4.6Zr in the physiological solution in the presence of joint lubricants.
2. The low corrosion rate in the range of 0.6–0.8 mm/year and high value of polarization resistance in the range of 3–5 ohm in physiological solution in the presence of joint lubricant demonstrate the potential of this material as biomaterials for joint application.
3. The electrochemical behaviour of Ti–29Nb–13Ta–4.6Zr alloy in physiological solution is not influenced by the nature of joint lubricant significantly. However, the growth of passive layer is the slowest and the passive layer is the most porous in Hank's solution containing HA. The corrosion rate is governed by diffusion of corroding species in the electrolyte in HBSS solution containing DPPC

References

1. Kim YW (1989) Intermetallic alloy based on gamma titanium aluminide. J Met 41:24–30
2. Long M, Rack HJ (1998) Titanium alloys in total joint replacement—a materials science perspective. Biomaterials 19:1621–1639
3. Jasty M (1993) Clinical reviews, particulate debris and failure of total hip replacement. J Appl Biomater 4:273–276
4. Zheng YF, Wang BL (2006) Mechanical properties and corrosion behaviour of beta titanium alloy. Key Eng Mater 324–325:695–698
5. Pan J, Thierry D, Leygraf C (1996) Electrochemical impendence spectroscopy study of passive oxide film on titanium for joint application. Electrochem Acta 41:1143–1153
6. Bălţatu S, Vizureanu P, Mareci D, Burtan LC, Chiruţă C, Trincă LC (2016) Effect of Ta on the electrochemical behavior of new TiMoZrTa alloys in artificial physiological solution simulating in vitro inflammatory conditions. Mater Corr 67(12):1314–1320
7. Khan MA, Williams RL (1999) The corrosion behavior of Ti-6Al-4V, Ti-6Al-7Nb and Ti-13Nb-13Zr in protein solutions. Biomaterials 20:631–667
8. Gonzalez JEG, Mirza Rosca JC (1999) Study of the corrosion behavior of titanium and some of its alloys for biomedical and dental implant applications. J Electroanal Chem 471:109–115
9. Lopez MF, Gutierrez A, Jimenez JA (2002) In vitro corrosion behavior of titanium alloys without vanadium. Electrochem Acta 47:1359–1364
10. Vasilescu C, Drob SI, Osiceanu P, Calderon-Moreno JM, Drob P, Vasilescu E (2015) Characterisation of passive film and corrosion behaviour of a new Ti-Ta-Zr alloy in artificial oral media: In time influence of pH and fluoride ion content. Mater Corr 66:971–981
11. Cvijović-Alagić I, Cvijović Z, Bajat J, Rakin M (2016) Electrochemical behavior of Ti-6Al-4V alloy with different microstructures in a simulated bio-environment. Mater Corr 67(10):1075–1087
12. Al-Mayauf AM, Al-Swayih AA, Al-Mobarak NA, Al-Jabab AS (2004) Corrosion behaviour of an new titanium alloy for dental implant applications influoride media. Mater Chem Phys 86:320–329
13. Narayanan R, Seshadri SK (2008) Point defect model and corrosion of anodic oxide coatings on Ti-6Al-4V. Corr. Sci 50:1521–1529
14. Ion R, Vasilescu C, Drob P, Vasilescu E, Cimpean A, Drob SI, Gordin DM, Gloriant T (2014) Long-term corrosion performances c Ti and Ti–6Al–4V alloy in severe functional conditions. Mater Corr 65(6):593–604
15. Shukla AK, Balasubramaniam R (2006) effect of surface treatment on electrochemical behavior of CP Ti, Ti-6Al-4V, Ti-13Nb-13Zr alloys in simulated body fluid. Corr Sci 48:1696–1720
16. Gordin DM, Gloriant T, Nemtoi GH, Chelariu R, Aelenei N, Guillou A, Ansel D (2005) Synthesis structure and electrochemical behaviour of beta Ti-12.5Mo alloy a new biomaterial. Mater Lett 59:2959–2964
17. Assis ASL, Wolynec S, Costa I (2006) Corrosion characterization of titanium alloys by electrochemical techniques. Electrochim Acta 51:1815–1819
18. Sahu S, Palaniappa M. Paul SN, Roy M (2010) Potentiodynamic behaviour of Ti alloys in physiological solution containing lubricant. Mater Lett 64:12–14

19. Arya SB, Bhattacharya A, Roy M (2018) Electrochemical corrosion behavior of Ti-10V-2Fe-3Al in different corrosive media, Mater Corr. https://doi.org/10.1002/maco.201709894

20. Tamilselvi S, Raman V, Rajendran S (2006) Corrosion behaviour of Ti-6Al-7Nb and Ti-6Al-4V alloys in the simulated body fluid solution by electrochemical impendence spectroscopy. Electrochem Acta 52:839–846

21. Alvarado CD, Sundaram PA (2006) Corrosion evaluation of Ti-48Al-2Cr-2Nb in Ringer solution. Acta Biomater 2:701–708

22. Diomidis N, Mischler S, More NS, Roy M (2012) Tribo-electrochemical characterization of metallic biomaterials for total joint replacement. Acta Biomater 8:852–859

23. Diomidis N, Mischler S, More NS, Roy M, Paul SN (2011) Fretting-corrosion behavior of titanium alloys in simulated synovial fluid. Wear 271:1093–1102

24. More NS, Diomidis N, Paul SN, Roy M, Mischler S (2011) Tribo-corrosion behavior of β titanium alloys in physiological solutions containing synovial components. Mater Sci Eng C 31:400–408

25. Milošev I, Kosec T, Strehblow HH (2008) XPS and EIS study of the passive film formed on orthopedic Ti-6Al-7Nb in Hank's physiological solution. Electrochim Acta 53:3547–3558

26. Stern M, Geary A (1957) Electrochemical polarization I. J Electrochem Soc 104:56–63

27. Meticos-Hukovic M. Kwokal A, Piljac J (2003) The influence of niobium and vanadium on passivity of titanium based implants in physiological solution. Biomaterials 24:3765–3775

28. Kobayashi E, Wang TJ, Doi H, Yoneyama T, Hamanaka H (1998) Mechanical properties and corrosion resistance of Ti-6Al-7Nb alloy dental casting.Mater. Sci Mater Med 9:567–574

29. Ganzalez JEG, Ruitz MDC, Rivarola JB, Pasquevich D (1998) Study of the corrosion behavior of titanium and some of its alloys for biomedical and dental implant applications. J Mater Sci 33:4173–4180

30. Vermilyea DA (1957) Nucleation of crystalline Ta_2O_5 during field crystallization. J Electrochem Soc 104:542–546

31. Leach JSL, Pearson BR (1988) Crystallization in anodic oxide films. Corr Sci 28:43–56

32. Laque FL, Copson HR (1963) Corrosion resistance of metals and alloys. Reinhold Publishing Corporation/Chapman & Hall Ltd, New York

33. Helsen JA, Breme J (1998) Metals as biomaterials. Wiley, Chichester

34. Lopez MF, Gutierrez A, Jimenez JA (2002) In vitro corrosion behavior of titanium alloys without vanadium. Electrochim Acta 47:1359–1364

35. Boukamp BA (1986) A nonlinear least square fit procedure for analysis of immittance data of electrochemical systems. Solid State Ionics 21:31–44

36. Tsuru T, Haruyama S, Gijutsu B (1978) Electrochemical corrosion properties of Ti–6Al–4V implant alloy in the biological environment. J. Japan Soc. Corr Eng 27:573–581

37. Fonseca C, Barbosa MA (2001) Corrosion behaviour of Ti in bio fluids containing H_2O_2 studied by electrochemical impendence spectroscopy. Corr Sci 43:547–559

38. Hsu RWW, Yang CC, Huang CA, Chen YS (2004) Electrochemical corrosion properties of Ti–6Al–4V implant alloy in the biological environment. Mater Sci Eng A 380:100–109

39. Alves VA, Reis RQ, Santos ICB, Souza DG, T de F Gonçalves, Pereira-da-Silva MA, Rossi A, da Silva LA (2009) In-situ impendence spectroscopy study of the electrochemical corrosion of Ti and Ti-6Al-4V in simulated body fluid at 25 °C and 37 °C. Corr. Sci 51:2473–2482

40. Raman V, Nagarajan S, Rajendran N (2006) electrochemical impedance spectroscopic characterization of passive film formed over β Ti- 29Nb-13Ta-4.6Zr. Electrochem. Commun 8:1309–1314